Available online at www.sciencedirect.com
SCIENCE DIRECT®
Coordination Chemistry Reviews 248 (2004) 1247–1257
COORDINATION CHEMISTRY REVIEWS
www.elsevier.com/locate/ccr

Review

Towards optimisation of electron transfer processes in dye sensitised solar cells

James R. Durrant*, Saif A. Haque, Emilio Palomares

Centre for Electronic Materials and Devices, Department of Chemistry, Imperial College, London SW7 2AZ, UK

Received 29 October 2003; accepted 9 March 2004
Available online 19 May 2004

Contents

Abstract 1247
1. Introduction 1247
2. Interfacial electron transfer dynamics 1248
   2.1. Theoretical considerations 1248
   2.2. TiO_2 density of states 1248
   2.3. Electron injection 1249
   2.4. Recombination dynamics 1250
   2.5. A model of interfacial electron transfer dynamics 1252
   2.6. Transport versus interfacial electron transfer limited recombination dynamics 1252
3. Control of the interfacial dynamics 1253
   3.1. Kinetic redundancy 1253
   3.2. Influence of dye protonation on the injection kinetics 1253
   3.3. Metal oxide blocking layers 1254
4. Concluding remarks 1256
Acknowledgements 1256
References 1256

Abstract

Studies of photoinduced charge separation in supermolecular systems, such as molecular diads, have shown that achieving a high yield of long lived and energetic charge separated states requires careful optimisation of system design. Such optimisation typically requires a compromise between conflicting constraints with, for example, increased electronic coupling favouring a high charge separation yield but at the expense of lifetime of the charge separated state. In this paper we will apply such considerations to the optimisation of interfacial electron transfer dynamics in dye sensitised, nanocrystalline solar cells, focusing on the dynamics of electron injection and charge recombination between sensitiser dyes and nanocrystalline TiO_2 electrodes. We will first of all review our fundamental understanding of these dynamics in terms of non-adiabatic electron transfer theory, and discuss the influence of electron trapping within the TiO_2 upon these dynamics. We will then go on to address what the 'optimum' electron transfer dynamics are for efficient device function, and in particular the concept of 'kinetic redundancy' whereby it is undesirable to have unnecessarily fast forward electron transfer reactions. We consider strategies to achieve optimum electron transfer dynamics, focusing in particular on the control of these dynamics by the use of conformal metal oxide coatings. Finally the fundamental limitations to optimisation of the interfacial electron transfer dynamics are discussed, addressing in particular the potential role of interfacial energetic inhomogeneities in limiting device optimisation.

Keywords: Dye sensitised; Photoelectrochemical; Solar cell; Electron transfer

1. Introduction

Interfacial electron transfer kinetics are critical to the function of dye sensitised solar cells [1,2]. Kinetic competition at the dye sensitised interface plays a central role in

* Corresponding author. Tel.: +44-20-7594-5321; fax: +44-20-7594-5801.
E-mail address: j.durrant@ic.ac.uk (J.R. Durrant).

0010-8545/$ – see front matter © 2004 Elsevier B.V. All rights reserved.
doi:10.1016/j.ccr.2004.03.014

determining device energy conversion efficiency. Efficient charge separation requires the electron injection kinetics (k_{inj}) to be faster than decay of the excited state decay to ground (k_0). Efficient cation transfer to the redox electrolyte requires the dye cation re-reduction by the redox couple (k_{reg}) to be faster than recombination between injected electrons and photogenerated dye cations (k_{cr}). Finally, efficient charge collection requires charge recombination between injected electrons and oxidised redox species in the electrolyte to be slower than transport of these species to the working and counter electrodes, respectively.

In this paper we focus upon the electron injection and recombination processes k_{inj} and k_{cr} observed following pulsed laser excitation of the dye sensitised nanocrystalline TiO_2 films:

$$D^* \overset{k_{inj}}{\rightarrow} D^+ + e^-_{MO} \quad (1)$$

$$D^+ + e^-_{MO} \overset{k_{cr}}{\rightarrow} D \quad (2)$$

In Section 2 of this paper we consider the parameters influencing these charge separation and recombination dynamics, and the extent to which these dynamics can be described by simple non-adiabatic electron transfer theory. In Section 3, we address strategies which can be employed to optimise these dynamics in dye sensitised solar cells, introducing the concept of 'kinetic redundancy', and suggesting that optimum device function will be obtained when the charge separation dynamics are just fast enough to compete effectively against excited state decay to ground. Two strategies are considered for optimisation of the charge separation and recombination dynamics: (1) variation of the protonation state of the sensitiser dye; and (2) the introduction of a high band-gap metal oxide barrier layer on the surface of the nanocrystalline TiO_2 film. In both sections we focus on nanocrystalline TiO_2 films sensitised by the $Ru(dcbpy)_2(NCS)_2$ dye (*cis*-bis (isothiocyanato)bis(2,2′-bipyridil-4,4′-dicarboxilato)-ruthenium(II)), these being the materials most typically employed in technological development of dye sensitised solar cells.

2. Interfacial electron transfer dynamics

2.1. Theoretical considerations

Following theoretical treatments of interfacial electron transfer processes developed in the 1960s, the rate constant k_{inj} for electron injection from the excited state of an adsorbed dye molecule into the conduction band of an electrode can be expressed as [3]:

$$k_{inj} = A \int V^2(1 - f(E, E_F))g(E) \times \exp\left(\frac{-(E_m - E + \lambda)^2}{4\lambda k_B T}\right) dE \quad (3)$$

where k_{inj} is the electron injection rate constant, V the electronic coupling between the dye excited state and each conduction band state of the electrode (assumed to be state independent) and E_m is the excited state oxidation potential energy of the adsorbed molecule. E is the electrochemical potential energy of conduction band states (and therefore negative for most semiconductors). The equation corresponds essentially to an extension of Marcus non-adiabatic electron transfer theory by incorporating a continuum of electronic states in the semiconductor. $g(E)$ is the normalised density of states of these electronic states, $f(E, E_F)$ is the Fermi occupancy factor to account of the fact that electron injection is only possible into unoccupied states. λ is the reorganisational energy associated with electron injection. The exponential term in this equation results in electron injection occurring optimally to conduction band states lying λ below the dye excited state energy, corresponding to activationless electron injection. A central prediction of this equation is that as the Fermi level (or conduction band edge) of the semiconductor is raised to an energy within $\sim\lambda$ of the dye excited state oxidation potential, the rate of electron injection is retarded. This retardation arises from the reduction in the number of unoccupied acceptor states available for electron injection. An analogous treatment can be made for the recombination reaction k_{cr} [3]. Such recombination reactions have been previously reported to lie in the Marcus inverted region, with a significant activation barrier to charge recombination [4].

From Eq. (1) it is apparent that the electron injection should ideally exhibit first order, exponential kinetics. Similarly from (2), second order dynamics should in general be expected for the recombination reaction k_{cr}. However we note that the density of electrons $[e^-_{MO}]$ may result not only from photoinjected electrons but also the density of electrons present in the metal oxide conduction band/sub-bandgap states prior to optical excitation, as defined by the position of the metal oxide Fermi level. The metal oxides under consideration here are n-type semiconductors. In the limit of low intensity optical excitation, and therefore a low density of photogenerated dye cations, the total electron density will be greater than the density of photogenerated dye cations ($[e^-_{MO}] \gg [D^+]$); under such conditions pseudo-first order recombination dynamics are expected.

2.2. TiO_2 density of states

The form of the TiO_2 density of states $g(E)$ is critical to evaluation of Eq. (3). A key consideration in experimental determination of $g(E)$ is that, due to the small diameter (approximately 15 nm) of the metal oxide nanoparticles comprising the film, $g(E)$ is strongly dependent upon the adsorption of charged species to the film surface. In particular, due to the protonation/deprotonation of surface bound hydroxyl groups, nanocrystalline TiO_2 films have been shown to exhibit Nernstein shifts of their conduction band energetics by 60 meV per pH unit [5–7]. Potential

determining ions for flat potential of such films have been shown to include not only protons but also small metal cations such as lithium [8,9]. Experimental probes of $g(E)$ in the presence of electrolytes have been largely limited to electrochemical and spectroelectrochemical studies of electron density $[e^-_{MO}]$ as a function of applied potential. Such experiments have, for example, exploited the characteristic blue/black coloration of nanocrystalline TiO_2 films at negative potentials attributed to the reduction of Ti^{4+} ions to Ti^{3+}. Such studies have typically found the electron density increases approximately exponentially with negative applied potential E_F:

$$[e^-_{MO}] \propto \exp\left(-\frac{E_F}{E_0}\right) \quad (4)$$

Typical experimental values for E_0 lie in the range 60–100 meV [10–12]. Assuming that $g(E)$ is independent of E_F, the observation that $E_0 > k_BT$ suggests these electrons do not primarily result from increased occupancy of the TiO_2 conduction band. This behaviour is however consistent with an exponentially increasing density of states:

$$g(E) \propto \exp\left(-\frac{E}{E_0}\right) \quad (5)$$

It has thus been concluded that nanocrystalline TiO_2 films exhibit an exponential tail of sub-bandgap states below their conduction band. These states are typically assigned to localised Ti^{3+} species.

2.3. Electron injection

Efficient charge separation requires the rate of electron injection to be faster than the decay of the dye excited state to ground. Following optical excitation of the main metal-to-ligand charge transfer transition of $Ru(dcbpy)_2(NCS)_2$ (absorption maximum at ~535 nm) in solution, a rapid relaxation (<150 fs) of this excited state results in the generation of a lower energy excited state [13], thought be of primarily triplet character, with a emission maximum at ~800 nm. Such behaviour is typical of ruthenium bipyrdyl dyes [14]. The lifetime of this excited state is 50 ns in degassed solvent [15], and 3–25 ns when absorbed to an inert substrate (ZrO_2) [13], indicating that achieving a high yield of electron injection will require electron injection time constants of 100 ps to 1 ns or faster.

The kinetics of charge separation for $Ru(dcbpy)_2(NCS)_2$ sensitised TiO_2 films have received extensive attention in recent years, with significant differences in the injection dynamics being reported by different studies [13,17–26]. Our own studies [13,18,20] of such films covered in an inert solvent (PC/EC) have reported non-exponential kinetics on timescales from <150 fs to tens or hundreds of picoseconds. Multiexponential analyses of such data have resolved components assigned to electron injection with lifetimes (relative amplitudes) of <100 fs (0.29), 1.0 ps (0.25) and 13 ps (0.46). Similar experiments reported elsewhere have resolved similar components, with the addition of a further component with lifetime of 100 ps [19]. Remarkably similar, multiexponential injection kinetics have been reported for a range of other sensitiser dyes adsorbed to nanocrystalline TiO_2 films, including zinc and free base tetracarboxyphenyl porphyrins (Zn and H_2 TCPP, respectively) [20] and fluorescin 27 [21,22]. We note that all of these dyes are expected to have excited state energies well above the TiO_2 conduction band edge and be bound such that the excited state is close to the TiO_2 surface. Studies of sensitiser dyes, for example, employing spacers between the dye excited state and the film surface have reported a significant retardation of the injection kinetics [23]. Several studies have focussed on the <100 fs phase of the electron injection dynamics, with the relative amplitude of this phase being found to increase as the excitation wavelength is shifted to shorter wavelengths and as the free energy difference between the dye excited state and the electrode conduction band edge is increased [24,25]. Both effects have been shown to be consistent with kinetic competition between ultrafast electron injection from the dye singlet excited state and energetic relaxation to the dye triplet state.

The non-exponential nature of the injection kinetics are clearly inconsistent with homogeneous, first order injection kinetics as expressed by Eq. (1). This non-exponentiality is not dye specific and therefore cannot be attributed solely to kinetic competition between electron injection and relaxation dynamics of the dye excited state. We [26] and others [16] have proposed that this non-exponential behaviour may derive from local inhomogeneities in density of acceptor states $g(E)$:

$$g_i(E) = g(E + d_i) \quad (6)$$

where the local density of states $g_i(E)$ of site i exhibits an energetic shift from the ensemble averaged density of states by an energy shift d_i. Shifts of the energetics of $g(E)$ have been suggested elsewhere to be the origin of variations in the yield [16,27] and kinetics [25,28] of electron injection for similar dye sensitised TiO_2 and ZnO films as a function of the concentration of potential determining ions in the electrolyte in which the film is immersed. Microscopically, local variations in surface charge can be expected to result in inhomogeneities in the density of acceptor states $g_i(E)$ for each dye molecule, as indicated in Eq. (6). Fig. 1 shows a comparison of numerical calculations using Eq. (3) and employing this inhomogeneous model with experimental injection data. The model calculations employ an exponential density of states as given in Eq. (5) and a Gaussian distribution of d_i with FWHM Δ. The nonexponential shape of the model calculations was determined by the value of the ratio Δ/E_0, with $\Delta/E_0 = 1.5$ providing the best fit to the data. Using a value of E_0 of 100 meV, typical of recent experimental observations, this yields a value of $\Delta = 150$ meV. This magnitude of inhomogeneous broadening seems reasonable, being for example of similar

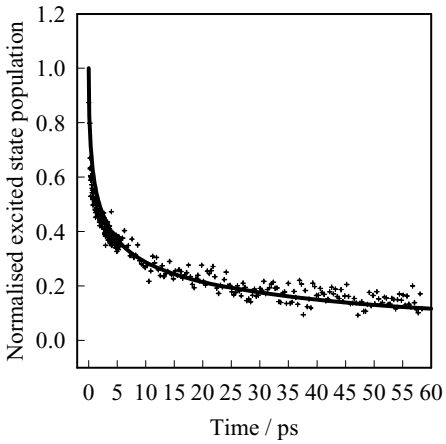

Fig. 1. Comparison of experimental electron injection kinetics (+) with model calculations (—) employing the inhomogeneous model with $(\Delta/E_0) = 1.5$. Data obtained from transient absorption data for $Ru(dcbpy)_2(NCS)_2/TiO_2$ films (+) covered in PC/EC (reproduced from [26]).

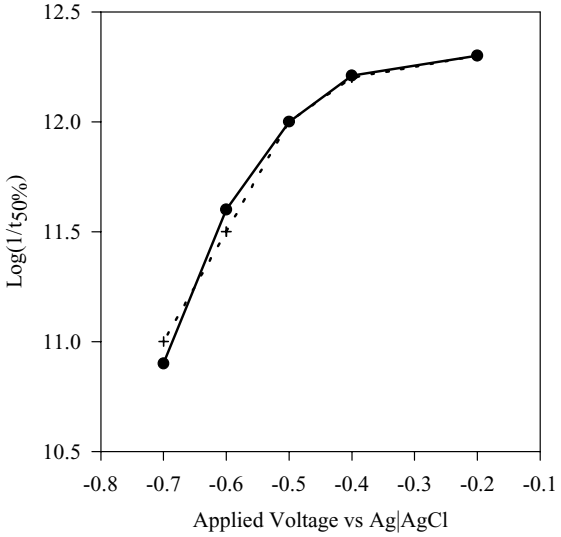

Fig. 2. Comparison of the electrical potential dependence of the half time for electron injection, $t_{50\%}$, observed experimentally (+) with that calculated from non-adiabatic electron transfer theory as given by Eq. (3) (⊕). Experimental data were obtained for a $Ru(dcbpy)_2(NCS)_2$ sensitised TiO_2 film in an MeCN/tetrabutyl ammonium perchlorate electrolyte. The best fit to the experimental data, as shown (○) yielded fitting parameters of $E_m = -0.75 \pm 0.05$ V vs. Ag/AgCl and $\lambda = 0.25 \pm 0.05$ eV (reproduced from [28]).

magnitude to the energetic distribution of chlorin radical pairs reported for photosynthetic reaction centres [29,30]. The energetic distribution observed in such pigment/protein complexes has also been attributed to inhomogeneities in the charge environment of individual pigments due to protonation/deprotonation of neighbouring groups (in this case amino acids rather than surface bound hydroxyl groups). Furthermore we have recently found experimental evidence for a similar inhomogeneous broadening in a study of the dye cation re-reduction (k_{reg}) employing a series of organic hole conductors [31]. This study was based on experimental measurement of the hole transfer yield from the dye cation to the hole conductor as a function of dye and hole conductor oxidation/ionisation potentials, and thereby as a function of reaction free energy. The experimental data were found be inconsistent with simple homogeneous equilibrium model, but consistent with an inhomogeneous model with $\Delta = 0.4$ eV. This study provides further evidence for significant energetic inhomogeneties at the TiO_2/dye/hole conductor interface, an issue we return to in Section 4 when we address fundamental limitations to device optimisation.

Following Eq. (3), the rate of electron injection is expected to be retarded as the Fermi level of the TiO_2 is raised, due to the acceptor states for electron injection become increasingly occupied. Fig. 2 shows a comparison of experimental data with model calculations addressing this issue [28]. Data were collected in a three electrode photoelectrochemcial cell, in which the sensitised film comprised the working electrode. Modulation of the potential applied to this electrode relative to the Ag/AgCl reference electrode results in modulation of the TiO_2 Fermi level. In these experiments, a full kinetic analysis of the injection dynamics was not possible as sufficient signal averaging was prevented by the limited stability of the sensitiser dye at negative potentials. Our analysis is therefore limited to consideration of the half time for electron injection ($t_{50\%}$) upon applied bias. It is apparent that the application of negative potentials results in a retardation of the injection kinetics by up to a factor 25. Model calculations employing Eq. (3) were found not be sensitive to the value of E_0 employed for $E_0 \geq 100$ meV. Such calculations provided a good fit to the experimental data, as shown in Fig. 2, with a value for the reorganisational energy $\lambda = 0.25 \pm 0.05$ eV.

In conclusion, we find that both the non-exponential nature of the electron injection dynamics observed for $Ru(dcbpy)_2(NCS)_2/TiO_2$ films, and their dependence upon electrode Fermi level, are consistent with non-adiabatic electron transfer theory, at least under the experimental conditions studied.

2.4. Recombination dynamics

Following electron injection into the TiO_2 film, the resulting charge separated state $D^+e^-_{MO}$ is remarkably stable, as illustrated in Fig. 3. Under the same experimental conditions as those employed in Fig. 1, the half time for charge recombination ($t_{50\%}$) is 0.4 ms. As for the injection kinetics, the recombination kinetics are non-exponential. They can be reasonably fit to a stretched exponential:

$$\Delta OD \propto \exp\left(-\left(\frac{t}{\tau}\right)^{\alpha}\right) \quad (7)$$

as illustrated in Fig. 3. Values of α obtained from such fits range from 0.25 to 0.5 dependent upon the electrolyte employed.

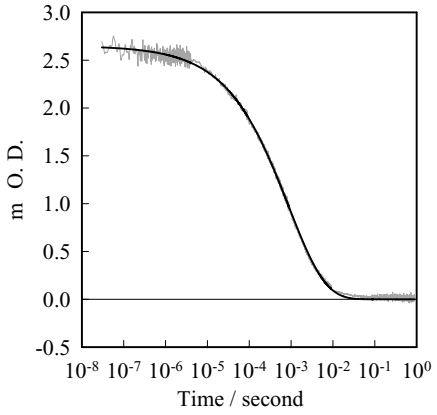

Fig. 3. Charge recombination dynamics for $Ru(dcbpy)_2(NCS)_2/TiO_2$ films covered in PC/EC, monitored by the decay of the dye cation absorption band at 800 nm. The smooth line is the best fit to the data employing a stretched exponential (Eq. (7)), with fit parameters of $\tau = 0.9$ ms and $\alpha = 0.5$ (adapted from [13]).

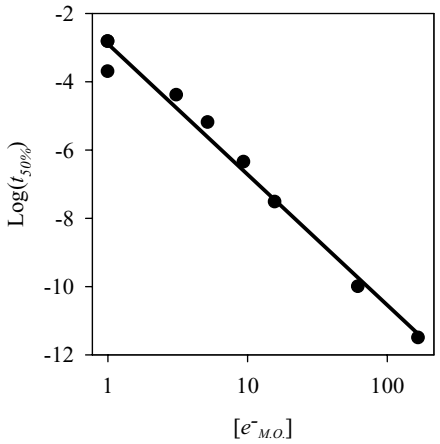

Fig. 4. Plot of the electron density $[e^-_{MO}]$ against the half time for charge recombination $t_{50\%}$ observed for a $Ru(dcbpy)_2(NCS)_2$ sensitised TiO_2 film in an ethanol/tetrabutyl ammonium perchlorate electrolyte. The electron density was modulated by varying the potential applied to the TiO_2 electrode in a three electrode photoelectrochemical cell. Electron densities were determined spectroelectrochemically in the absence of absorbed dyes. Recombination half times were determined by transient absorption spectroscopy (adapted from [32,33]).

Following Eq. (2), the recombination dynamics are expected to be first order in electron density $[e^-_{MO}]$. Experimental studies have indeed confirmed a strong dependence of the recombination dynamics upon electron density [32]. Studies in which $[e^-_{MO}]$ was increased by the application of a negative potential to the TiO_2 electrode resulted in rapid acceleration of the recombination kinetics. Shifting the applied potential from +0.1 V versus Ag/AgCl to −0.8 V resulted in an acceleration of recombination half time, $t_{50\%}$, by $\sim 10^8$ from 1 ms to ~3 ps. Similarly studies conducted at a constant applied potential, but in which $[e^-_{MO}]$ was modulated by employing different electrolyte solutions to vary $g(E)$, resulted in variations in $t_{50\%}$ by up to 10^6. However these dependencies are too large to be consistent with a first order dependence of $t_{50\%}$ upon $[e^-_{MO}]$. The lower limit for $[e^-_{MO}]$ in these experiments, observed for example at positive applied potentials, is the electron density generated by the laser pulse, corresponding to approximately one electron per nanoparticle. A linear dependence of recombination rate upon electron density would therefore require electron densities of up to 10^8 per nanoparticle, which is clearly implausible. We further note that as the recombination process is thought to occur in the Marcus inverted region ($|\Delta G| > \lambda$), a more detailed consideration employing non-adiabatic electron transfer theory would result in a sub-linear dependence of $t_{50\%}$ upon $[e^-_{MO}]$, in even greater contrast with the experimental observations, and clearly indicating that the observed dependence of the recombination dynamics upon the Fermi level of the TiO_2 electrode can not be explained in terms of non-adiabatic electron transfer theory.

Fig. 4 shows a quantitative analysis of the dependence of the half time for charge recombination, $t_{50\%}$, upon electron density $[e^-_{MO}]$. For this plot, $[e^-_{MO}]$ was determined independently by spectroelectrochemical studies of steady state film optical density as a function of applied potential, employing the characteristic Ti^{3+} absorption associated with e^-_{MO} in TiO_2. It is apparent that $t_{50\%}$ exhibits a power law dependence upon $[e^-_{MO}]$:

$$t_{50\%} \propto [e^-_{MO}]^{-\beta} \tag{8}$$

where $\beta = 2$–4 dependent upon electrolyte employed. This behaviour is clearly inconsistent with a simple rate law first order in $[e^-_{MO}]$.

It has recently been shown that these experimental observations are consistent with a model in which the recombination process is primarily controlled not by the rate of interfacial electron transfer as expressed by Eq. (3), but by the dynamics of electron transport within the TiO_2 electrode [33,34]. The model, developed from the continuous time random walk model of Scher and Montroll [35], is based upon a random walk of electron between an energetic distribution of trap sites in the film. Each step of the random walk requires thermal excitation of the trapped electron up to the conduction band, and therefore is dependent upon the trap depth. The non-linear dependence of the recombination kinetics upon $[e^-_{MO}]$ results from the increased mobility of the electrons as the film Fermi level is raised, as increasingly shallow trap become occupied. The model furthermore predicts that, for an exponential density of states, the fitting parameters α and β of Eqs. (7) and (8) obtained from analyses of experimental data for different electrolytes should be related by:

$$a = \frac{1}{\beta} \tag{9}$$

This correlation is in good agreement with experimental observations for a range of different electrolytes, providing further support for the validity of this model [32,33].

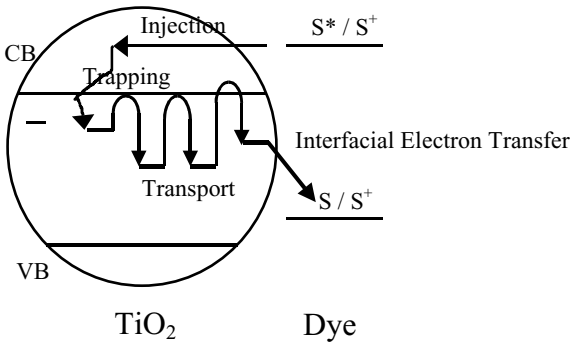

Fig. 5. Illustration of model of electron injection and charge recombination in dye sensitised nanocrystalline TiO_2 films (reproduced from [36]).

2.5. A model of interfacial electron transfer dynamics

A model of the interfacial dynamics for dye sensitised nanocrystalline TiO_2 films consistent with the experimental observations discussed above is illustrated in Fig. 5. Following optical excitation of the $Ru(dcbpy)_2(NCS)_2$ sensitiser dye, an electron is injected from the dye excited state into acceptor states of the semiconductor. The non-exponential kinetics observed for this process, and their dependence upon TiO_2 Fermi level, are consistent with non-adiabatic electron transfer theory. The injection proceeds primarily on timescales slower than relaxation of the dye excited state. The half-time for electron injection is, in the absence of applied bias, ~0.4 ps, although the injection kinetics are non-exponential, with a significant proportion occurring on timescales >100 ps.

Following electron injection, the electron relaxes to localised sub-band gap states associated with localised Ti^{3+} formation. Subsequent charge recombination requires thermal detrapping of this electron and motion through the TiO_2 film until it sufficiently close to an oxidised dye molecule such that the direct electron transfer is possible. The recombination dynamics are controlled by the total density of electrons in the film, with electrons injected by electrical bias and optical photoinjection yielding similar recombination behaviour, indicating that the initially injected electron does not appear to remain adjacent to or associated with its corresponding dye cation. The electron motion within the TiO_2 film can be well described by the CTRW model, corresponding to anomalous diffusion of electrons through an energetic distribution of trap sites [33].

2.6. Transport versus interfacial electron transfer limited recombination dynamics

As illustrated in Fig. 5, the charge recombination dynamics observed following pulsed laser excitation may be described by two distinct processes, electron transport through the TiO_2 particles to a location adjacent to the dye cation, and then an interfacial electron transfer step from the TiO_2 to the dye. In principle, depending upon the relative rate constants for these two processes, either may limit the overall recombination dynamics. The CTRW model discussed above focuses on the electron transport dynamics and is therefore valid in the limit when the interfacial electron transfer step is fast relative to the transport dynamics. We have recently demonstrated [36] that, by suitable design of the sensitiser dye, it is possible to move from this transport limited regime to a regime in which the recombination dynamics are limited by the electron transfer step, as illustrated in Fig. 6. By employing a triphenyl amine substituted porphyrin dye, we were able to retard the interfacial electron transfer step sufficiently such that this step rate limits the overall charge recombination process. As a consequence, the temporal shape of the recombination dynamics exhibits a transition from the stretched exponential behaviour assigned above to transport limited recombination, to a monoexponential decay consistent with pseudo first order behaviour following Eq. (2) with $[e^-_{MO}] \gg [D^+]$.

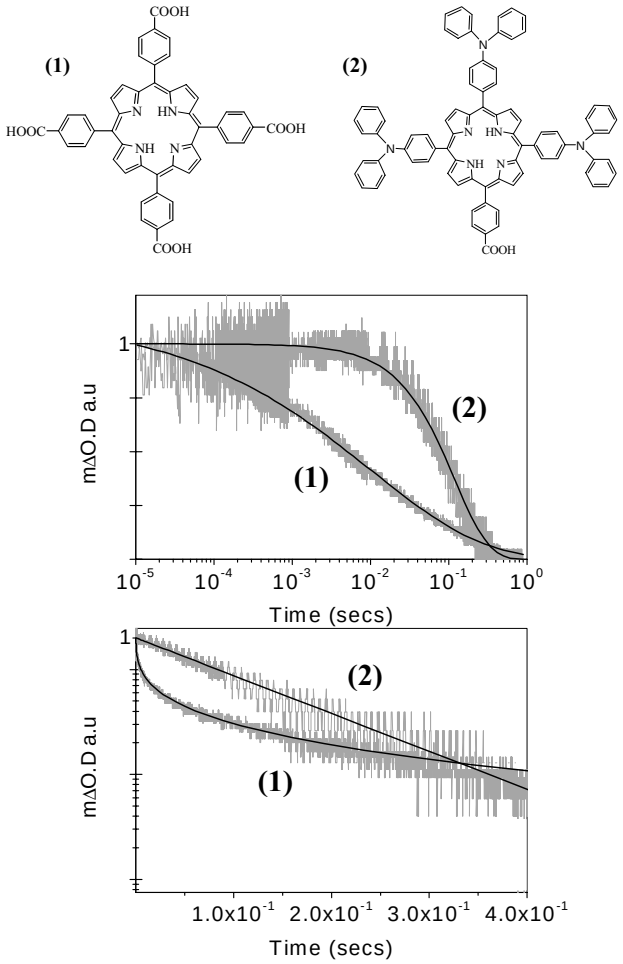

Fig. 6. Transient absorption data monitoring charge recombination dynamics for TiO_2 films sensitised with dye 1 and dye 2 (structures shown in upper (a)). Both figures are the same data, with (b) being a lin/log plot and (c) being a log/lin plot. The black lines are the fits to the decay kinetics corresponding to (1) a stretched exponential ($\Delta OD \propto \exp[-(t/\tau)^{\alpha}]$, $\alpha = 0.31$) and (2) a monoexponential decay (reproduced from [36]).

More recently we have also shown similar transitions between stretched exponential, transport limited recombination to monoexponential, interfacial electron transfer limited recombination for a range of other experimental systems, including electron transfer from TiO_2 to the iodine/iodide redox couple [37], and interfacial charge recombination through metal oxide barrier layers.

3. Control of the interfacial dynamics

3.1. Kinetic redundancy

Efficient device operation requires the photogeneration of a high yield of a long lived interfacial charge separated state. Such light driven charge separation dynamics have been extensively studied in homogeneous supramolecular structures, such as donor/acceptor diads suspended in solution [38–40]. Such studies have shown that the dynamics of charge separation and recombination are closely related, with for example modulation of the electronic coupling between the donor and acceptor having equal effects upon both the charge separation and recombination dynamics. Moreover variation of the energetics of charge separation results in modulation of not only the charge separation dynamics, but also modulation of recombination dynamics both to the diad ground and excited states. Optimisation of diad performance therefore requires careful consideration of all reaction dynamics, with for example 'optimised' electronic coupling being a compromise between it being sufficiently large such that charge separation competes effectively with excited state decay, whilst being sufficiently small to minimise charge recombination.

The considerations employed in this analysis of molecular diads can be applied to the dye sensitised TiO_2 interface. In this case the system is more complex due to the band of electron acceptor states in the TiO_2, resulting in more complex relationships between the reaction dynamics and their corresponding electronic coupling and energetics, as discussed in Section 3. Not withstanding this more complex behaviour, the conclusion remains the same—namely that the dynamics of electron injection and recombination are closely related, and that, without the introduction of secondary electron transfer steps, any attempt to modulate one process will invariably modulate both. In practice for DSSC, it is critical to minimise charge recombination dynamics both to the oxidised dyes and to the redox couple in the electrolyte. It follows from the arguments above that attempts to minimise this recombination will typically also impact on the charge separation dynamics. Device optimisation therefore requires optimisation of the system such as to minimise the recombination dynamics whilst maintaining electron injection dynamics which are just sufficient to achieve a high yield of charge separation. In this context, an optimised device will most probably not exhibit ultrafast injection dynamics, but rather only injection dynamics fast compared with excited state decay, in agreement with a recent 'two level system' analysis of molecular cells [41]. Given that for $Ru(dcbpy)_2(NCS)_2$ the excited state decay dynamics are 10–50 ns, optimum injection dynamics will most probably be on the timescale of 100 ps to 1 ns. As such ultrafast (sub-picosecond) injection dynamics are 'kinetically redundant', and indeed an indicator of a poorly optimised system.

In practice, optimisation of DSSC is at present a largely empirical process, often based on iterative changes in the device composition and fabrication procedures. Such attempts at device optimisation typically find an inverse correlation between the device short circuit current and open circuit voltage, with improvements in one tending to be at the expense of the other. This inverse correlation can be readily rationalised, at least qualitatively, in terms of the analysis discussed above, with minimisation of the recombination dynamics resulting in increased open circuit voltage, but at the expense of slower charge separation dynamics and therefore short circuit current.

3.2. Influence of dye protonation on the injection kinetics

We first of all exemplify the concept of kinetic redundancy by comparison of the electron injection dynamics observed for nanocrystalline TiO_2 films sensitised by the fully protonated version of $Ru(dcbpy)_2(NCS)_2$ dye (often referred to as 'N3') and its di-tetrabutyl ammonium salt $(TBA)_2Ru(dcbpy)_2(NCS)_2$ (often referred to as 'N719'). Kinetic studies of electron injection, as discussed in Section 2.2 above, have largely employed the fully protonated dye N3. However in functioning devices, the N719 dye has been found to give a higher device open circuit voltage, partially offset by a lower short circuit current, and overall superior device efficiency. This difference in performance has been attributed to the influence of dye protonation upon the energetics of the TiO_2 conduction band, with the less protonated N719 dye resulting in a more negative conduction band edge, and thereby a high open circuit voltage [42].

We have compared the kinetics of electron injection for the N719 and N3 sensitiser dyes adsorbed to nanocrystalline TiO_2 films, as shown in Fig. 7. It is apparent that the di-TBA salt N719 exhibits electron injection dynamics 30 fold slower than the fully protonated N3 dye. This retardation is consistent with the expected influence of dye protonation on the TiO_2 electron acceptor state energetics, and consistent with a recent study of injection dynamics as a function of the pH environment of the film [25]. In the context of 'kinetic redundancy' it is noteworthy that the dye yielding the slower injection dynamics yields the more efficient overall device performance. For both dyes the injection dynamics remain fast relative to excited state decay to ground, such that the 30-fold retardation has only a marginal effect upon the yield of electron injection. More important for device function is the concomitant effect on the recombination dynamics, with the lower film protonation reducing the film electron density at a given cell potential, thereby

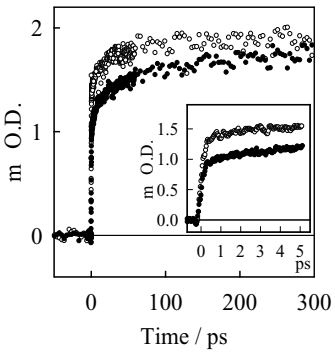

Fig. 7. Transient absorption kinetics for nanocrystalline TiO_2 films sensitised by the fully protonated dye N3 (open circles) and its di-TBA salt N719 (filled circles). Data was collected at probe wavelength of 760 nm employing excitation at 595 nm. The samples were covered in PC/EC. The inset shows an expansion of the data at early times (reproduced from [18]).

reducing recombination losses and increasing the cell open circuit potential.

3.3. Metal oxide blocking layers

One approach to modulating the electronic coupling between the TiO_2 and the sensitiser dye is to introduce metal oxide barriers layers between these two species. Several groups have reported approaches to the deposition of such conformal blocking layers. As some examples, Tennakone and co-workers have reported the preparation of MgO-coated SnO_2 films by the hydrolysis of magnesium acetate using high temperatures or by the use of metal chlorides such as $AlCl_3$ to fabricate Al_2O_3 coated SnO_2 photoelectrodes [43–47]. Zaban and co-workers [48,49] prepared a Nb_2O_5 coated TiO_2 film under argon-controlled atmosphere using 2-propanol niobium isopropoxide solution and sintering at 500 °C while Kay and Gratzel [50] improved the efficiency of SnO_2 based solar cells with different metal oxide barrier layers such as Y_2O_3.

We have developed a surface hydrolysis process based on stepwise adsorption of metal alkoxides to achieve the conformal growth of metal oxide blocking layers [51,52]. In this technique, the metal alkoxide is chemisorbed on a hydroxylated TiO_2 nanoporous metal oxide film, washed in adequate solvents and then either heated at high temperature or water rinsed to achieve complete hydrolysis of the precursor and form the insulator layer, as illustrated in Fig. 8. The TiO_2 films were immersed by dipping each film in a solution of suitable precursors, followed by sintering at 450 °C for 20 min in order to complete the hydrolysis. Fig. 9 illustrates HRTEM images of TiO_2 nanoparticles before and after depositing an Al_2O_3 overlayer, indicating a control over the conformal growth of the Al_2O_3 obtaining a film thickness of 9 ± 1 Å. The overlayer thickness is dependent upon the precursor concentration in the dipping solution, but largely independent of the dipping time and temperature. Overlayer thickness could readily be increased by repeating their dipping/sintering cycle.

The primary function of such conformal growth of blocking layers in DSSC is to increase the physical separation of injected electrons and oxidized dye, thereby retarding the recombination reactions. Such conformal coating film are analogous to binary core/shell nanoparticles [53], where electronically insulating shell layers are grown on nanoparticles in solution to shield the core material of the nanoparticles from the external environment. However for the DSSC, it is preferable that the coating is conducted conformally upon the preformed metal oxide film; the fabrication of films from pre-coated core/shell nanoparticles can be expected to result in insulating barriers between the nanoparticles, impeding efficient electron transport through the film. We

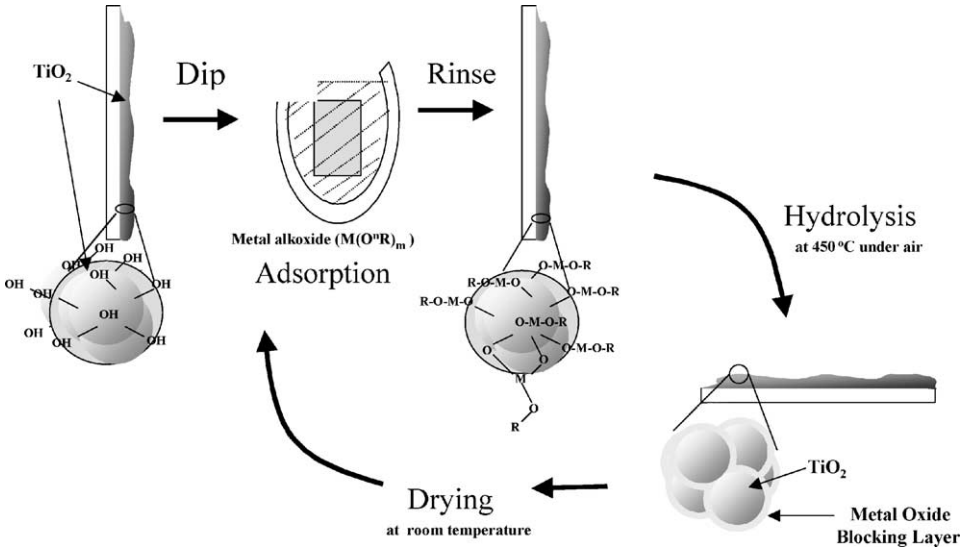

Fig. 8. Illustration of the coating process. A typical dipping procedure involves immersion of the TiO_2 film in 15 mM ethanolic solution of the alkoxide for 10 min at room temperature.

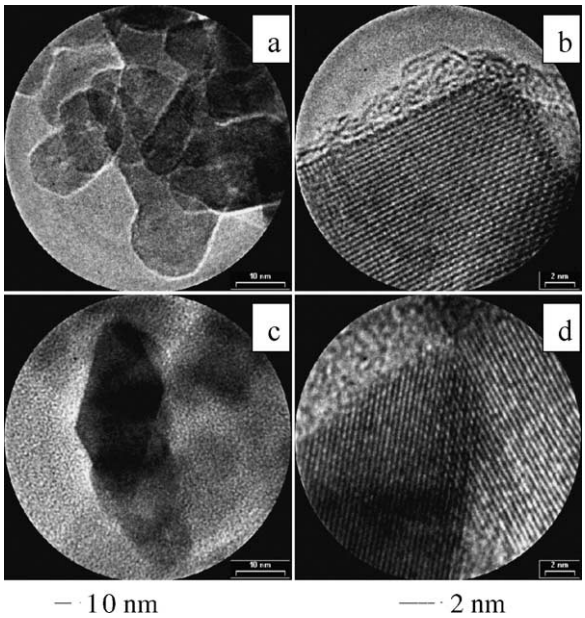

Fig. 9. HRTEMs of TiO_2 nanoparticles in presence (a, b) and absence (c, d) of an Al_2O_3 overlayer. The Al_2O_3 overlayer was grown conformally on a preformed nanocrystalline TiO_2. This film, and the uncoated control, was then broken up to a powder to allow HRTEM analysis. Pictures (b) and (d) are at high magnification. Image (a) clearly illustrates the Al_2O_3 overlayer (apparent as a white line) conformally coating each TiO_2 nanoparticle. Image (b) indicates a overlayer thickness of 900 ± 100 Å nm (reproduced from [52]).

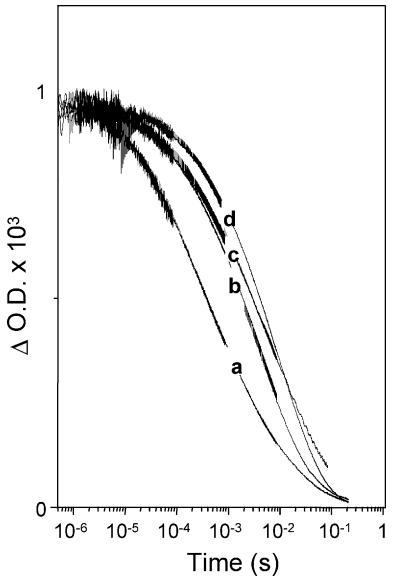

Fig. 10. Transient absorption data monitoring photoinduced absorption of the $RuL_2(NCS)_2$ cation following optical excitation of this dye adsorbed on nanoporous: (a) TiO_2; (b) Al_2O_3/TiO_2; (c) SiO_2/TiO_2; and (d) ZrO_2/TiO_2 photoelectrodes. The signal decay is assigned to charge recombination of the dye cation with electrons in trap/conduction band states of the TiO_2 semiconductor. Optical excitation was at 630 nm, and detection at 800 nm (reproduced from [52]).

furthermore note that such blocking layers will also retard the desired interfacial charge separation reaction, although due the 'kinetic redundancy' discussed above, a modest reduction in the charge separation dynamics can be achieved without loss of charge separation yield and therefore device efficiency. Careful control of blocking layer thickness is therefore essential to allow optimum retardation of the recombination dynamics, whilst retaining a yield of photoinduced electron injection.

Fig. 10 shows typical transient absorption spectroscopy data for TiO_2 films coated with three different metal oxide overlayers and then sensitised with the N719 dye. It is apparent that overlayers of ZrO_2, Al_2O_3 and SiO_2 all result in significant retardation of the recombination dynamics relative to the uncoated control, consistent with the expected blocking layer function of these materials. It is furthermore apparent that the electron injection yield, monitored by the initial amplitude of the cation absorption signal, is essentially unaffected by these overlayers. Increasing the overlayer thickness by repeating the dipping cycle resulted in further retardation of the recombination dynamics, but at the expense of a loss of the initial dye cation signal, and an increase in dye photoluminescence, indicating that thicker overlayers result in a retardation of the electron injection dynamics to such an extent that they no longer compete successfully with dye excited-state decay [52].

Whilst all three metal oxide overlayers resulted in retardation of the recombination dynamics in the absence of applied bias, their behaviour under external bias control is very distinct, as shown in Fig. 4. At positive applied biases, both Al_2O_3 and SiO_2 overlayers resulted in a approximately two-fold retardation of the recombination dynamics, consistent with the data shown in Fig. 11. However, under negative bias, the Al_2O_3 coated film exhibits only weak dependence of the recombination dynamics upon applied bias.

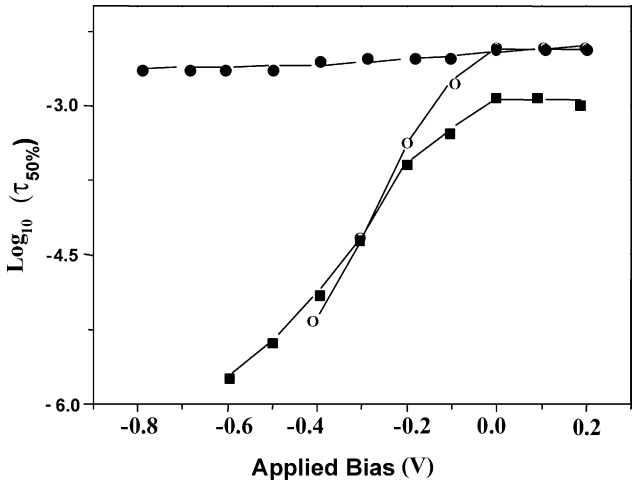

Fig. 11. Dependence of the half time for charge recombination $t_{50\%}$ upon applied bias (vs. a Ag/AgCl electrode reference) for $RuL_2(NCS)_2$ sensitized (■) TiO_2; (○) SiO_2/TiO_2; and (●) Al_2O_3/TiO_2 films. $t_{50\%}$ data obtained from transient absorption decays analogous to those shown in Fig. 10 collected as a function of applied bias in a three electrode photoelectrochemical cell with redox inactive electrolyte (reproduced from [52]).

In contrast the SiO_2 coated film exhibits an enhanced bias dependence relative to the uncoated control, and for biases <-0.3 V actually exhibits faster recombination dynamics than the uncoated control. Correlation with chronoamperometric studies indicates this behaviour can be rationalized in terms of the influence of the acid/base properties of the overlayer upon the electron density of the TiO_2 film, with the more basic Al_2O_3 overlayer serving to raise the TiO_2 conduction band, thereby minimising the increase in electron density and therefore the acceleration of the recombination dynamics under negative biases. Overall, the retardation of the recombination dynamics resulting from the Al_2O_3 overlayer results in a 50 mV increase in the cell open circuit voltage and an increase to device efficiency by up to 35%. It can be concluded that such blocking layers impact on device performance in two ways: as a physical barrier to increase the dye: TiO_2 spatial separation and as a flat band determining treatment, modulating the electron density within the TiO_2 at a given film Fermi level.

4. Concluding remarks

In this review we have addressed the parameters that play an important role in influencing the charge separation and recombination reactions in dye sensitised nanocrystalline titanium dioxide solar cells. We have then gone on to discuss strategies that can be employed to optimise these dynamics in dye sensitised solar cells. Optimum device function, and specifically optimum device open circuit voltage, requires minimisation of interfacial charge recombination dynamics. Such minimisation however typically results in retardation of the charge separation dynamics, and if taken too far results in a loss of charge separation yield and therefore device short circuit current. In practice, device optimisation often involves a suitable compromise between these two conflicting constraints. As such optimum device performance requires the avoidance of any 'kinetic redundancy', with the charge separation dynamics being just fast enough to achieve a high charge separation yield.

We have exemplified our argument of kinetic redundancy by two strategies employed to optimise device performance: variation of the protonation state of the sensitiser dye, and the introduction of a metal oxide barrier layer on the surface of the nanocrystalline TiO_2 film. Both strategies are based upon the premise that the ultrafast (sub-picosecond) injection kinetics observed for the fully protonated $Ru(dcbpy)_2(NCS)_2$ adsorbed directly to TiO_2 electrodes are kinetically redundant, being three to four orders of magnitude faster than the competing excited state decay to ground. In the former case, deprotonation of two carboxylate groups of the dye resulted in slower charge separation dynamics, and improved device performance. In the latter case, the insertion of metal oxide barrier layers was observed to retard both the charge separation and recombination dynamics, and again an improved device performance.

Building further upon the analogy with molecular diads discussed in Section 3, it is well established that an attractive route to increasing the lifetime of a charge separated state while minimising any loss of yield or stored free energy is the use of secondary electron donors and acceptors. As such, optimum performance for molecular systems has been achieved by the use of pentads comprising a relay of five redox species [54]. This strategy is of course also the basis of the electron transfer relays found in photosynthetic reaction centres. The use of intermediate redox moieties is therefore a potentially attractive route to optimisation of DSSC. The success of such strategies is however critically dependent upon retaining the spatial separation of the charges, in the context of liquid electrolyte DSSCs such strategies may be of only limited applicability due to the pervasive diffusion of the iodide/tri-iodide redox couple.

On a more fundamental level, optimisation of the kinetics and energetics of the interfacial electron transfer dynamics in DSSC can be achieved most efficiently for homogeneous systems. Energetic inhomogeneities result in the need for larger mean free energy differences to achieve high reaction yields. Similarly, in the context of kinetic competition, non-exponential injection dynamics result in the need for a faster mean injection time constant to achieve a high injection yield. As such the non-exponential dynamics and energetic inhomogeneities apparent in the experimental data discussed above may provide significant limitations to device performance, and, unless removed, may ultimately limit optimisation of the energy conversion efficiency of dye sensitised solar cells.

Acknowledgements

The authors would like to thank their co-workers for many useful and helpful discussions, including in particular Jenny Nelson and David Klug. Financial support from the EPSRC is gratefully acknowledged. Dr. E. Palomares is also pleased to acknowledge the financial support from the European Union (Marie Curie European Fellowship Contract No. HPMF-CT-2002-01744).

References

[1] A. Hagfeldt, M. Gratzel, Acc. Chem. Res. 33 (2000) 269.
[2] N. Kopidakis, K.D. Benkstein, J. van de Lagemaat, A.J. Frank, J. Phys. Chem. B 107 (2003) 11307.
[3] W. Schmickler, Interfacial Electrochemistry, Oxford University Press, Oxford, 1996.
[4] D. Kuciasuskas, M.S. Freund, H.B. Gray, J.R. Winkler, N.S. Lewis, J. Phys. Chem. B 105 (2001) 392.
[5] G. Rothenberger, D. Fitzmaurice, M. Gratzel, J. Phys. Chem. B 96 (1992) 5983.
[6] M. Gratzel, Curr. Opin. Colloid Interface Sci. 4 (1999) 314.
[7] A. Zaban, S. Ferrer, J. Sprague, B.A. Gregg, J. Phys. Chem. B 101 (1997) 55.
[8] G. Redmond, D. Fitzmaurice, J. Phys. Chem. B 97 (1993) 1426.

[9] F. Fabregat-Santiago, I. Mora-Sero, G. Garcia-Belmonte, J. Bisquert, J. Phys. Chem. B 107 (2003) 758.
[10] N.W. Duffy, L.M. Peter, R.M.G. Rajapakse, K.G.U. Wijayantha, Electrochem. Commun. (2000) 2.
[11] R.L. Willis, C. Olson, B. O'Regan, T. Lutz, J. Nelson, J.R. Durrant, J. Phys. Chem. B 106 (2002) 7605.
[12] A. Kay, M. Gratzel, J. Phys. Chem. B 97 (1993) 6272.
[13] Y. Tachibana, J.E. Moser, M. Gratzel, D.R. Klug, J.R. Durrant, J. Phys. Chem. 100 (1996) 20056.
[14] N.H. Damraurer, G. Cerullo, A. Yeh, T.R. Boussie, C.V. Shank, J.K. McCusker, Science 275 (1997) 54.
[15] M.K. Nazeeruddin, A. Kay, I. Rodicio, R. Humphry-Baker, E. Muller, P. Liska, N. Vlachopolous, M. Gratzel, J. Am. Chem. Soc. 115 (1993) 6382.
[16] R. Katoh, A. Furube, K. Hara, S. Murata, H. Sugihara, H. Arakawa, M. Tachiya, J. Phys. Chem. B 106 (2002) 12957.
[17] J. Kallioinen, G. Benko, V. Sundstrom, J. Korppi-Tommola, A.P. Yartsev, J. Phys. Chem. B 106 (2002) 4396.
[18] Y. Tachibana, M.K. Nazeeruddin, M. Gratzel, D.R. Klug, J.R. Durrant, Chem. Phys. 285 (2002) 127.
[19] J. Kallioinen, V. Lehtovuori, P. Myllyperkio, J. Korppi-Tommola, Chem. Phys. Lett. 340 (2001) 217.
[20] Y. Tachibana, S.A. Haque, I.P. Mercer, D.R. Klug, J.R. Durrant, J. Phys. Chem. B 104 (2000) 1198.
[21] G. Benko, M. Hilgendorff, A.P. Yartsev, V. Sundstrom, J. Phys. Chem. B 105 (2001) 967.
[22] N.J. Chepery, G.P. Smestad, M. Gratzel, J.Z. Zhang, J. Phys. Chem. B 101 (1997) 9342.
[23] J.B. Asbury, E. Hao, W. Wang, T. Lian, J. Phys. Chem. B 104 (2000) 11957.
[24] G. Benko, J. Kallioinen, J. Korppi-Tommola, A.P. Yartsev, V. Sundstrom, J. Am. Chem. Soc. 124 (2002) 489.
[25] J.B. Asbury, N.A. Anderson, X. Ai, E. Hao, T. Lian, J. Phys. Chem. B 107 (2003) 7376.
[26] Y. Tachibana, I.V. Rubstov, I. Montari, K. Yoshikara, D.R. Klug, J.R. Durrant, J. Photochem. Photobiol. A: Chem. 142 (2001) 215.
[27] C.A. Kelly, F. Farzad, D.W. Thompson, J.M. Stipkala, G.J. Meyer, Langmuir 15 (1999) 7047.
[28] Y. Tachibana, S.A. Haque, I.P. Mercer, J.E. Moser, D.R. Klug, J.R. Durrant, J. Phys. Chem. B 105 (2001) 7424.
[29] M-L. Groot, E.J.G. Petermann, P.J.M. vanKan, I.H.M. vanStokkum, J.P. Dekker, R. vanGrondelle, Biophys. J. 67 (1994) 318.
[30] A. Ogrodnik, W. Keupp, M. Volk, G. Aumeier, M.E. Michelbeyerle, J. Phys. Chem. 98 (1994) 3432.
[31] S.A. Haque, T. Park, A.B. Holmes, J.R. Durrant, Chem. Phys. Chem. 1 (2003) 89.
[32] S.A. Haque, Y. Tachibana, R.L. Willis, J.E. Moser, M. Gratzel, D.R. Klug, J.R. Durrant, J. Phys. Chem. B 104 (2000) 538.
[33] (a) J. Nelson, S.A. Haque, D.R. Klug, J.R. Durrant, Phys. Rev. B 63 (2001) 5321;
(b) J. Nelson, Phys. Rev. B 59 (1999) 15374.
[34] A.V. Barzykin, M. Tachiya, J. Phys. Chem. B 106 (2002) 4356.
[35] H. Scher, E.W. Montroll, Phys. Rev. B 12 (1975) 2455.
[36] J.N. Clifford, G. Yahioglu, L.R. Milgrom, J.R. Durrant, Chem. Commun. (2002) 1260.
[37] S.A. Haque, J. Nelson, J.R. Durrant, Proceedings of the Electrochemical Society, ECS, 2001, p. 138.
[38] S. Fukuzumi, Org. Biomol. Chem. 1 (2003) 609.
[39] R. Lomoth, T. Haupl, O. Johansson, L. Hammarstrom, Chem. Eur. J. 8 (2002) 102.
[40] H. Yamada, H. Imahori, Y. Nishimura, I. Yamakazi, T. Kyu Ahn, S. Keun Kim, D. Kim, S. Fukuzumi, J. Am. Chem. Soc. 125 (2003) 9129.
[41] J. Nelson, J. Kirkpatrick, J. Appl. Phys. A 79 (2004) 15.
[42] M.K. Nazeeruddin, S.M. Zakeeruddin, R. Humphry-Baker, M. Jirousek, P. Liska, N. Vlachopoulos, V. Shlover, C.H. Fisher, M. Gratzel, Inorg. Chem. 38 (1999) 6298.
[43] G.R.R.A. Kumara, K. Tennakone, V.P.S. Perera, A. Konno, S. Kaneko, M. Okuya, J. Phys. D: Appl. Phys. 34 (2001) 868.
[44] K. Tennakone, V.P.S. Perera, I.R.M. Kottegoda, G.R.R.A. Kumara, J. Phys. D: Appl. Phys. 32 (1999) 374.
[45] K. Tennakone, G.R.R.A. Kumara, I.R.M. Kottegoda, V.P.S. Perera, Chem. Commun. (1999) 15.
[46] K. Tennakone, P.K.M. Bandaranayake, P.V.V. Jayaweera, A. Konno, G.R.R.A. Kumara, Physica E 14 (2002) 190.
[47] K. Tennakone, J. Bandara, P.K.M. Bandaranayake, G.R.R.A. Kumara, A. Konno, Jpn. J. Appl. Phys. 40 (2001) L732.
[48] Y. Diamant, S.G. Chen, O. Melamed, A. Zaban, J. Phys. Chem. B 107 (2003) 1977.
[49] S.G. Chen, S. Chappel, Y. Diamant, A. Zaban, Chem. Mater. 13 (2001) 4629.
[50] A. Kay, M. Gratzel, Chem. Mater. 14 (2002) 2930.
[51] E. Palomares, J.N. Clifford, S.A. Haque, T. Lutz, J.R. Durrant, Chem. Commun. (2002) 1464.
[52] E. Palomares, J.N. Clifford, S.A. Haque, T. Lutz, J.R. Durrant, J. Am. Chem. Soc. 125 (2003) 475.
[53] L. Han, D.R. Daniel, M.M. Maye, C. Zhong, Anal. Chem. 73 (2001) 4441.
[54] L. de la Garza, J. Goojin, P.A. Liddell, T. Sotomura, T.A. Moore, A.L. Moore, D. Gust, J. Phys. Chem. B 107 (2003) 10252.